

Study of Doubly Strange Systems using Stored Antiprotons

The PANDA Collaboration

B. Singh^a, W. Erni^b, B. Krusche^b, M. Steinacher^b, N. Walford^b, B. Liu^c, H. Liu^c, Z. Liu^c, X. Shen^c, C. Wang^c, J. Zhao^c, M. Albrecht^d, T. Erlen^d, M. Fink^d, F. Heinsius^d, T. Held^d, T. Holtmann^d, S. Jasper^d, I. Keshk^d, H. Koch^d, B. Kopf^d, M. Kuhlmann^d, M. Kümmel^d, S. Leiber^d, M. Mikirtychyants^d, P. Musiol^d, A. Mustafa^d, M. Pelizäus^d, J. Pychy^d, M. Richter^d, C. Schnier^d, T. Schröder^d, C. Sowa^d, M. Steinke^d, T. Triffterer^d, U. Wiedner^d, M. Ball^e, R. Beck^e, C. Hammann^e, B. Ketzer^e, M. Kube^e, P. Mahlberg^e, M. Rossbach^e, C. Schmidt^e, R. Schmitz^e, U. Thoma^e, M. Urban^e, D. Walther^e, C. Wendel^e, A. Wilson^e, A. Bianconi^{f,be}, M. Bragadireanu^g, M. Caprini^g, D. Pantea^g, B. Patel^h, W. Czyzyckiⁱ, M. Domagalaⁱ, G. Filoⁱ, J. Jaworowskiⁱ, M. Krawczykⁱ, E. Lisowskiⁱ, F. Lisowskiⁱ, M. Michałekⁱ, P. Poznańskiⁱ, J. Płazekⁱ, K. Korcyl^j, A. Kozela^j, P. Kulesa^j, P. Lebedowicz^j, K. Pysz^j, W. Schäfer^j, A. Szczurek^j, T. Fiutowski^k, M. Idzik^k, B. Mindur^k, D. Przyborowski^k, K. Swientek^k, J. Biernat^l, B. Kamys^l, S. Kistryn^l, G. Korcyl^l, W. Krzemien^l, A. Magiera^l, P. Moskal^l, A. Pyszniak^l, Z. Rudy^l, P. Salabura^l, J. Smyrski^l, P. Strzempek^l, A. Wronska^l, I. Augustin^m, R. Böhm^m, I. Lehmann^m, D. Nicmorus Marinescu^m, L. Schmitt^m, V. Varentsov^m, M. Al-Turanyⁿ, A. Beliasⁿ, H. Deppeⁿ, R. Dzhygadloⁿ, A. Ehretⁿ, H. Flemmingⁿ, A. Gerhardtⁿ, K. Götzenⁿ, A. Gromliukⁿ, L. Gruberⁿ, R. Karabowiczⁿ, R. Kliemtⁿ, M. Krebsⁿ, U. Kurillaⁿ, D. Lehmannⁿ, S. Löchnerⁿ, J. Lühningⁿ, U. Lynenⁿ, H. Orthⁿ, M. Patsyukⁿ, K. Petersⁿ, T. Saitoⁿ, G. Schepersⁿ, C.J. Schmidtⁿ, C. Schwarzⁿ, J. Schwieningⁿ, A. Täschnerⁿ, M. Traxlerⁿ, C. Ugurⁿ, B. Vossⁿ, P. Wiczorekⁿ, A. Wilmsⁿ, M. Zühlsdorfⁿ, V.M. Abazov^o, G. Alexeev^o, A. Arefiev^o, V.I. Astakhov^o, M.Yu. Barabanov^o, B.V. Batyunya^o, Yu.I. Davydov^o, V.Kh. Dodokhov^o, A.A. Efremov^o, A. Fechtchenko^o, A.G. Fedunov^o, A. Galoyan^o, S. Grigoryan^o, E.K. Koshurnikov^o, V.I. Lobanov^o, Y.Yu. Lobanov^o, A.F. Makarov^o, L.V. Malinina^o, V.L. Malyshev^o, A. Olshevskiy^o, E. Perevalova^o, A.A. Piskun^o, T. Pocheptsov^o, G. Pontecorvo^o, V. Rodionov^o, Y. Rogov^o, R. Salmin^o, A. Samartsev^o, M.G. Sapozhnikov^o, G. Shabratova^o, N.B. Skachkov^o, A.N. Skachkova^o, E.A. Stokovsky^o, M. Suleimanov^o, R. Teshev^o, V. Tokmenin^o, V. Uzhinsky^o, A. Vodopyanov^o, S.A. Zaporozhets^o, N.I. Zhuravlev^o, A.G. Zorin^o, D. Branford^p, D. Glazier^p, D. Watts^p, M. Böhm^q, A. Britting^q, W. Eyrich^q, A. Lehmann^q, M. Pfaffinger^q, F. Uhlig^q, S. Dobbs^r, K. Seth^r, A. Tomaradze^r, T. Xiao^r, D. Bettoni^s,

V. Carassiti^s, A. Cotta Ramusino^s, P. Dalpiaz^s, A. Drago^s, E. Fioravanti^s, I. Garzia^s, M. Savriè^s, V. Akishina^t, I. Kisel^t, G. Kozlov^t, M. Pugach^t, M. Zyzak^t, P. Gianotti^u, C. Guaraldo^u, V. Lucherini^u, A. Bersani^v, G. Bracco^v, M. Macri^v, R.F. Parodi^v, K. Biguenko^w, K. Brinkmann^w, V. Di Pietro^w, S. Diehl^w, V. Dormenev^w, P. Drexler^w, M. Düren^w, E. Etzelmüller^w, M. Galuska^w, E. Gutz^w, C. Hahn^w, A. Hayrapetyan^w, M. Kesselkaul^w, W. Kühn^w, T. Kuske^w, J.S. Lange^w, Y. Liang^w, V. Metag^w, M. Nanova^w, S. Nazarenko^w, R. Novotny^w, T. Quagli^w, S. Reiter^w, J. Rieke^w, C. Rosenbaum^w, M. Schmidt^w, R. Schnell^w, H. Stenzel^w, U. Thöring^w, M. Ullrich^w, M.N. Wagner^w, T. Wasem^w, B. Wohlfarth^w, H. Zaunick^w, D. Ireland^x, G. Rosner^x, B. Seitz^x, P.N. Deepak^y, A. Kulkarni^y, A. Apostolou^z, M. Babai^z, M. Kavatsyuk^z, P. Lemmens^z, M.Lindemulder^z, H. Loehner^z, J. Messchendorp^z, P. Schakel^z, H. Smit^z, M. Tiemens^z, J.C. van der Weele^z, R. Veenstra^z, S. Vejdani^z, K. Dutta^{aa}, K. Kalita^{aa}, A. Kumar^{ab}, A. Roy^{ab}, H. Sohlbach^{ac}, M. Bai^{ad}, L. Bianchi^{ad}, M. Büscher^{ad}, L. Cao^{ad}, A. Cebulla^{ad}, R. Dossdall^{ad}, A. Gillitzer^{ad}, F. Goldenbaum^{ad}, D. Grunwald^{ad}, A. Hertel^{ad}, Q. Hu^{ad}, G. Kemmerling^{ad}, H. Kleines^{ad}, A. Lehrach^{ad}, R. Nellen^{ad}, H. Ohm^{ad}, S. Orfanitski^{ad}, D. Prasuhn^{ad}, E. Prencipe^{ad}, J. Pütz^{ad}, J. Ritman^{ad}, S. Schadmand^{ad}, T. Sefzick^{ad}, V. Serdyuk^{ad}, G. Sterzenbach^{ad}, T. Stockmanns^{ad}, P. Wintz^{ad}, P. Wüstner^{ad}, H. Xu^{ad}, A. Zambanini^{ad}, S. Li^{ae}, Z. Li^{ae}, Z. Sun^{ae}, H. Xu^{ae}, V. Rigato^{af}, L. Isaksson^{ag}, P. Achenbach^{ah}, O. Corell^{ah}, A. Denig^{ah}, M. Distler^{ah}, M. Hoek^{ah}, A. Karavdina^{ah}, W. Lauth^{ah}, Z. Liu^{ah}, M. Martínez Rojo^{ah,2}, H. Merkel^{ah}, U. Müller^{ah}, J. Pochodzalla^{ah,*}, S. Schlimme^{ah}, C. Sfienti^{ah}, M. Thiel^{ah}, H. Ahmadi^{ai}, S. Ahmed^{ai}, S. Bleser^{ai,1}, L. Capozza^{ai}, M. Cardinali^{ai}, A. Dbeyssi^{ai}, M. Deiseroth^{ai}, F. Feldbauer^{ai}, M. Fritsch^{ai}, B. Fröhlich^{ai}, P. Jasinski^{ai}, D. Kang^{ai}, D. Khanef^{ai}, R. Klasen^{ai}, H.H. Leithoff^{ai}, D. Lin^{ai}, F. Maas^{ai}, S. Maldaner^{ai}, M. Marta^{ai}, M. Michel^{ai}, M.C. Mora Esp^{ai}, C. Morales Morales^{ai}, C. Motzko^{ai}, F. Nerling^{ai}, O. Noll^{ai}, S. Pflüger^{ai}, A. Pitka^{ai}, D. Rodriguez Pieiro^{ai}, A. Sanchez Lorente^{ai}, M. Steinen^{ai,1}, R. Valente^{ai}, T. Weber^{ai}, M. Zambrana^{ai}, I. Zimmermann^{ai}, A. Fedorov^{aj}, M. Korjik^{aj}, O. Missevitch^{aj}, A. Boukharov^{ak}, O. Malyshev^{ak}, I. Marishev^{ak}, P. Balanutsa^{al}, V. Balanutsa^{al}, V. Chernetsky^{al}, A. Demekhin^{al}, A. Dolgolenko^{al}, P. Fedorets^{al}, A. Gerasimov^{al}, V. Goryachev^{al}, V. Chandratre^{am}, V. Datar^{am}, D. Dutta^{am}, V. Jha^{am}, H. Kumawat^{am}, A.K. Mohanty^{am}, A. Parmar^{am}, B. Roy^{am}, G. Sonika^{am}, C. Fritzschn^{an}, S. Grieser^{an}, A.K. Hergemöller^{an}, B. Hetz^{an}, N. Hüsken^{an}, A. Khoukaz^{an}, J. P. Wessels^{an}, K. Khosonthongkee^{ao}, C. Kobdaj^{ao}, A. Limphirat^{ao}, P. Srisawad^{ao}, Y. Yan^{ao}, M. Barnyakov^{ap}, A.Yu. Barnyakov^{ap}, K. Beloborodov^{ap}, A.E. Blinov^{ap}, V.E. Blinov^{ap}, V.S. Bobrovnikov^{ap}, S. Kononov^{ap}, E.A. Kravchenko^{ap}, I.A. Kuyanov^{ap}, K. Martin^{ap}, A.P. Onuchin^{ap}, S. Serebnyakov^{ap}, A. Sokolov^{ap}, Y. Tikhonov^{ap}, E. Atomssa^{aq}, R. Kunne^{aq}, D. Marchand^{aq}, B. Ramstein^{aq}, J. Van de Wiele^{aq}, Y. Wang^{aq}, G. Boca^{ar}, S. Costanza^{ar}, P. Genova^{ar}, P. Montagna^{ar}, A. Rotondi^{ar}, V. Abramov^{as}, N. Belikov^{as}, S. Bukreeva^{as}, A. Davidenko^{as}, A. Derevschikov^{as}, Y. Goncharenko^{as}, V. Grishin^{as}, V. Kachanov^{as}, V. Kormilitsin^{as}, A. Levin^{as}, Y. Melnik^{as}, N. Minaev^{as}, V. Mochalov^{as}, D. Morozov^{as},

L. Nogach^{as}, S. Poslavskiy^{as}, A. Ryazantsev^{as}, S. Ryzhikov^{as}, P. Semenov^{as}, I. Shein^{as},
A. Uzunian^{as}, A. Vasiliev^{as}, A. Yakutin^{as}, E. Tomasi-Gustafsson^{at}, U. Roy^{au}, B. Yabsley^{av},
S. Belostotski^{aw}, G. Gavrilov^{aw}, A. Izotov^{aw}, S. Manaenkov^{aw}, O. Miklukho^{aw},
D. Veretennikov^{aw}, A. Zhdanov^{aw}, K. Makonyi^{ax}, M. Preston^{ax}, P. Tegner^{ax},
D. Wölbing^{ax}, T. Bäck^{ay}, B. Cederwall^{ay}, A.K. Rai^{az}, S. Godre^{ba}, D. Calvo^{bb}, S. Coli^{bb},
P. De Remigis^{bb}, A. Filippi^{bb}, G. Giraud^{bb}, S. Lusso^{bb}, G. Mazza^{bb}, M. Mignone^{bb},
A. Rivetti^{bb}, R. Wheadon^{bb}, F. Balestra^{bc}, F. Iazzi^{bc}, R. Introzzi^{bc}, A. Lavagno^{bc},
J. Olave^{bc}, A. Amoroso^{bd}, M.P. Bussa^{bd}, L. Busso^{bd}, F. De Mori^{bd}, M. Destefanis^{bd},
L. Fava^{bd}, L. Ferrero^{bd}, M. Greco^{bd}, J. Hu^{bd}, L. Lavezzi^{bd}, M. Maggiora^{bd},
G. Maniscalco^{bd}, S. Marcello^{bd}, S. Sosio^{bd}, S. Spataro^{bd}, R. Birsa^{be}, F. Bradamante^{be},
A. Bressan^{be}, A. Martin^{be}, H. Calen^{bf}, W. Ikegami Andersson^{bf}, T. Johansson^{bf},
A. Kupsc^{bf}, P. Marciniowski^{bf}, M. Papenbrock^{bf}, J. Pettersson^{bf}, K. Schönning^{bf},
M. Wolke^{bf}, B. Galnander^{bg}, J. Diaz^{bh}, V. Pothodi Chackara^{bi}, A. Chlopik^{bj}, G. Kesik^{bj},
D. Melnychuk^{bj}, B. Slowinski^{bj}, A. Trzcinski^{bj}, M. Wojciechowski^{bj}, S. Wronka^{bj},
B. Zwieglinski^{bj}, P. Bühler^{bk}, J. Marton^{bk}, D. Steinschaden^{bk}, K. Suzuki^{bk}, E. Widmann^{bk},
J. Zmeskal^{bk},

and

Jürgen Gerlⁿ, Ivan Kojouharovⁿ, Jasmina Kojouharova^{bl}

^aAligarh Muslim University, Physics Department, Aligarh, India

^bUniversität Basel Switzerland

^cInstitute of High Energy Physics, Chinese Academy of Sciences, Beijing China

^dUniversität Bochum, I. Institut für Experimentalphysik, Germany

^eRheinische Friedrich-Wilhelms-Universität Bonn, Germany

^fUniversità di Brescia, Italy

^gInstitutul National de C&D pentru Fizica si Inginerie Nucleara "Horia Hulubei", Bukarest-Magurele, Romania

^hP.D. Patel Institute of Applied Science, Department of Physical Sciences, Changa India

ⁱUniversity of Technology, Institute of Applied Informatics, Cracow, Poland

^jIFJ, Institute of Nuclear Physics PAN, Cracow Poland

^kAGH, University of Science and Technology, Cracow, Poland

^lInstytut Fizyki, Uniwersytet Jagiellonski, Cracow, Poland

^mFAIR, Facility for Antiproton and Ion Research in Europe, Darmstadt, Germany

ⁿGSI Helmholtzzentrum für Schwerionenforschung GmbH, Darmstadt Germany

^oVeksler-Baldin Laboratory of High Energies (VBLHE), Joint Institute for Nuclear Research, Dubna Russia

^pUniversity of Edinburgh United Kingdom

^qFriedrich Alexander Universität Erlangen-Nürnberg, Germany

^rNorthwestern University, Evanston, U.S.A.

^sUniversità di Ferrara and INFN Sezione di Ferrara, Ferrara, Italy

^tFrankfurt Institute for Advanced Studies, Frankfurt Germany

^uINFN Laboratori Nazionali di Frascati, Italy

^vINFN Sezione di Genova, Italy

^wJustus Liebig-Universität Gießen II. Physikalisches Institut, Germany

^xUniversity of Glasgow, United Kingdom

^yBirla Institute of Technology and Science - Pilani, K.K. Birla Goa Campus, Goa, India

^zKVI-Center for Advanced Radiation Technology (CART), University of Groningen, Groningen, Netherlands

^{aa}Gauhati University, Physics Department, Guwahati, India

^{ab}Indian Institute of Technology Indore, School of Science, Indore, India

^{ac}Fachhochschule Südwestfalen Iserlohn, Germany

^{ad}Forschungszentrum Jülich, Institut für Kernphysik, Jülich, Germany

^{ae}Chinese Academy of Science, Institute of Modern Physics, Lanzhou, China

^{af}INFN Laboratori Nazionali di Legnaro, Italy

^{ag}Lunds Universitet, Department of Physics, Lund, Sweden

^{ah}Johannes Gutenberg-Universität, Institut für Kernphysik, Mainz, Germany



^{ai}Helmholtz Institute Mainz 55099 Mainz, Germany

^{aj}Research Institute for Nuclear Problems, Belarus State University, Minsk, Belarus

^{ak}Moscow Power Engineering Institute, Moscow, Russia

^{al}Institute for Nuclear Physics, Obninsk, Russia

^{am}Nuclear Physics Division, Bhabha Atomic Research Centre, Mumbai, India

^{an}Westfälische Wilhelms-Universität Münster, Germany

^{ao}Suranaree University of Technology, Nakhon Ratchasima, Thailand

^{ap}Budker Institute of Nuclear Physics of Russian Academy of Science, Novosibirsk, Russia

^{aq}Institut de Physique Nucléaire d'Orsay (UMR8608), CNRS/IN2P3 and Université Paris-Sud, 91406, Orsay cedex, France

^{ar}Dipartimento di Fisica, Università di Pavia, INFN Sezione di Pavia, Pavia, Italy

^{as}Institute for High Energy Physics, Protvino, Russia

^{at}IRFU, SPHN, CEA Saclay, Saclay, France

^{au}Sikaha-Bhavana, Visva-Bharati, WB, Santiniketan, India

^{av}S University of Sydney, School of Physics, Sydney, Australia

^{aw}National Research Centre "Kurchatov Institute" B.P. Konstantinov Petersburg Nuclear Physics Institute, Gatchina, St. Petersburg, Russia

^{ax}Stockholms Universitet, Stockholm Sweden

^{ay}Kungliga Tekniska Högskolan, Stockholm, Sweden

^{az}Sardar Vallabhbhai National Institute of Technology, Applied Physics Department, Surat, India

^{ba}Veer Narmand South Gujarat University, Department of Physics, Surat, India

^{bb}INFN Sezione di Torino, Torino, Italy

^{bc}Politecnico di Torino and INFN Sezione di Torino, Torino, Italy

^{bd}Università di Torino and INFN Sezione di Torino, Torino, Italy

^{be}Università di Trieste and INFN Sezione di Trieste, Trieste, Italy

^{bf}Uppsala Universitet, Institutionen för fysik och astronomi, Uppsala, Sweden

^{bg}The Svedberg Laboratory, Uppsala, Sweden

^{bh}Instituto de Física Corpuscular (IFIC) Universidad de Valencia - CSIC, Paterna, Valencia, Spain

^{bi}Sardar Patel University, Physics Department, Vallabh Vidyanagar, India

^{bj}National Centre for Nuclear Research, Warsaw, Poland

^{bk}Österreichische Akademie der Wissenschaften, Stefan Meyer Institut für Subatomare Physik, Wien, Austria

^{bl}Technische Hochschule Mittelhessen, 61169 Friedberg, Germany

Abstract

Bound nuclear systems with two units of strangeness are still poorly known despite their importance for many strong interaction phenomena. Stored antiproton beams in the GeV range represent an unparalleled factory for various hyperon-antihyperon pairs. Their outstanding large production probability in antiproton collisions will open the floodgates for a series of new studies of systems which contain two or even more units of strangeness at the PANDA experiment at FAIR. For the first time, high resolution γ -spectroscopy of doubly strange $\Lambda\Lambda$ -hypernuclei will be performed, thus complementing measurements of ground state decays of $\Lambda\Lambda$ -hypernuclei at J-PARC or possible decays of particle unstable hypernuclei in heavy ion reactions. High resolution spectroscopy of multi-strange Ξ^- -atoms will be feasible and even the production of Ω^- -atoms will be within reach. The latter might open the door to the $|S|=3$ world in strangeness nuclear physics, by the study of the hadronic Ω^- -nucleus interaction. For the first time it will be possible to study the behaviour of Ξ^+ in nuclear systems under well controlled conditions.

© 2016 Published by Elsevier Ltd.

Keywords: strangeness, hypernuclei, hyperatoms, antiprotons

1. Where QCD meets Gravity

One of the biggest challenges for physics in this century will be the unification of the four known fundamental forces within a common theoretical framework. Pure, matter-free strong-field gravity can be studied when black holes merge and gravitational waves are emitted [1]. Eventually, precise observations of gravitational waves will

*Corresponding author.

Email address: pochodza@kph.uni-mainz.de (J. Pochodzalla)

¹Part of doctoral thesis.

²Part of master thesis.

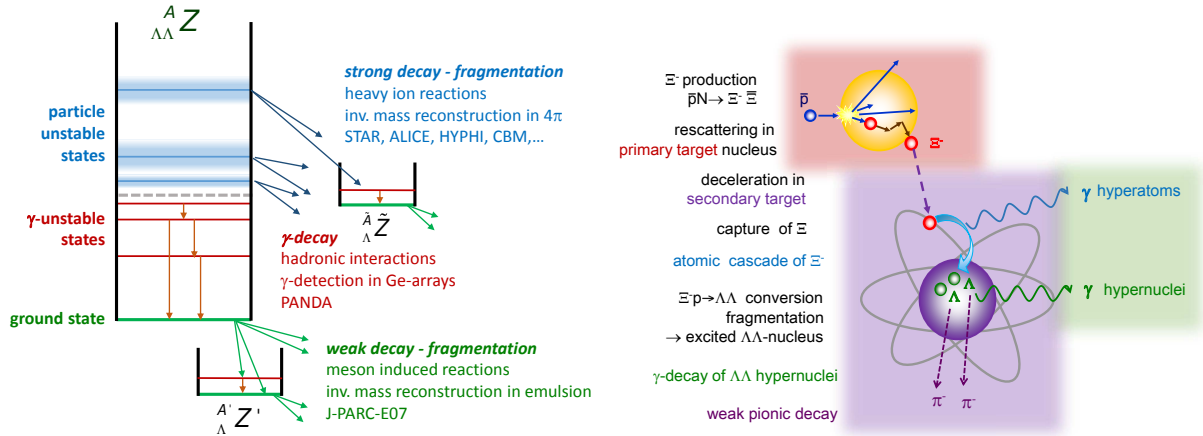


Figure 1. Left: Various decays which allow to study the level scheme of $\Lambda\Lambda$ -hypernuclei. Right: Production scheme of Ξ^- -hyperatoms and $\Lambda\Lambda$ -hypernuclei at PANDA.

constrain or even refute theories of modified gravity in the strong-field regime. Similar strong gravitational fields are also at work in compact stellar object, called neutron stars [2]. However, the formation of neutron stars are influenced by all four known fundamental forces. Their destiny is determined by the equation of state (EoS). The well understood electromagnetic interaction plays a minor role for their EoS and the weak interaction only enters indirectly by introducing additional hadronic degrees-of-freedom when high densities are approached. Therefore, neutron stars are unique cosmic laboratories to study the interplay between the strong QCD force on one side and gravity on the other side in extreme conditions which are not accessible by any other objects in the universe [2].

The recent observation of massive neutron stars with about twice the solar mass [3, 4] and the expected appearance of hyperons at about two times nuclear density remains an unresolved mystery in neutron stars (hyperon puzzle). At present, our incomplete understanding of the underlying baryon-baryon and of even more subtle multi-body interactions in baryonic systems seems to be the most probable reason for this dilemma. As an alternative solution to this puzzle the role of gravity has been questioned [5–7]. In the future, gravitational waves from merging neutron stars might help to probe gravity in this high density regime. The complementary study of the strong force in these objects and the determination of the EoS remains even after many decades of research one of the biggest challenge for physics. High energy nuclear reactions, radioactive beams mapping the chart of nuclear stability and precision studies of nuclear few body systems contribute to this task. Strangeness nuclear physics with its many facets is an essential protagonist in this big adventure.

Bound strange systems - hypernuclei as well as hyperatoms - represent unique laboratories for multi-baryon interactions in the strangeness sector. The confirmation of the substantial charge symmetry breaking in the $J=0$ ground states of the $A=4$ mirror hypernuclei ${}^4_{\Lambda}\text{H}$ and ${}^4_{\Lambda}\text{He}$ by precision measurements at MAMI [8] and at J-PARC [9] making use of novel techniques demonstrates impressively the necessity to combine complementary methods in strangeness nuclear physics [10]. The case of $\Lambda\Lambda$ -hypernuclei is another example for the need for such a cooperation (Fig. 1, left). Complex hypernuclear systems incorporating two hyperons can be studied by the E07 Collaboration at J-PARC using kaon beams [11], in antiproton-nucleus interactions in PANDA at FAIR [12], in massive nucleus-nucleus collisions [13–15] in the CBM and NUSTAR experiments at FAIR, STAR at RHIC [16] and ALICE at CERN [17]. Because of the two-step production mechanism of $\Lambda\Lambda$ -hypernuclei, spectroscopic studies based on two-body kinematics cannot be performed and spectroscopic information can only be obtained via their decay products. Experiments at J-PARC using kaon beams and nuclear emulsions will provide precise information on the absolute ground state masses of $\Lambda\Lambda$ -hypernuclei. Obviously, information on excited states can not be extracted from emulsion experiments. In principle also the kinetic energies of weak decay products are sensitive to the binding energies of the two Λ hyperons. While the double pionic decay of light $\Lambda\Lambda$ -hypernuclei can be used as an effective filter to reduce the background as it is foreseen at PANDA, the unique identification of hypernuclei ground states exclusively via their pionic decay in counter experiments is usually hampered by the limited momentum resolution (see e.g. [18]). The spectrum of ex-

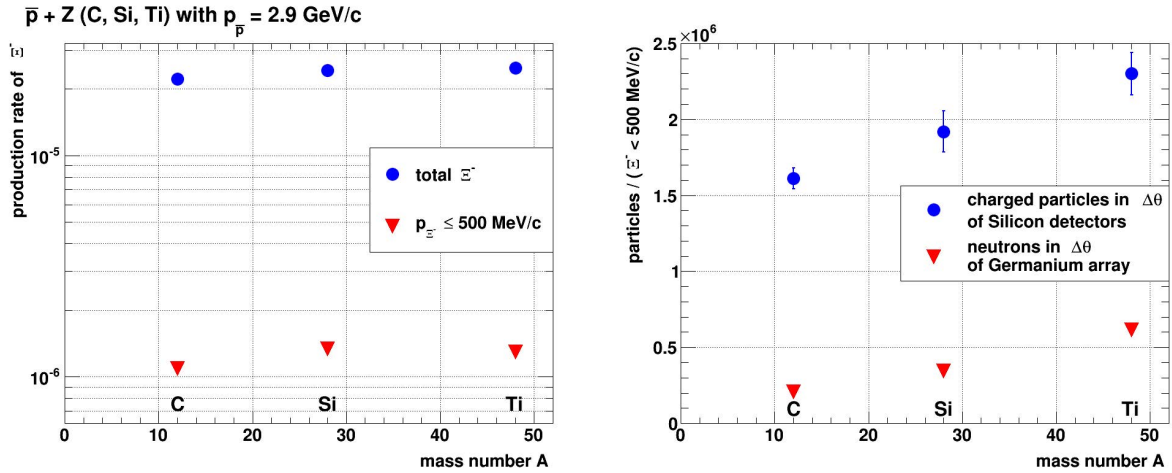


Figure 2. Left: Production probability of Ξ^- (blue dots) and Ξ^- with momenta below 500 MeV/c (red triangles) predicted by GiBUU simulations for 2.9 GeV/c \bar{p} interactions with three possible target materials. Right: Produced charged particles within the angular range covered by the silicon detectors of the secondary target (blue circles) and neutrons in the acceptance of the Germanium array (red triangles) normalized to the number of Ξ^- with momenta less than 500 MeV/c.

cited particle stable states will be explored at the PANDA experiment by performing high resolution γ -spectroscopy. Finally, two-particle correlation studies between Λ -hypernuclei and Λ hyperons similar to conventional two particle correlation studies in heavy ion reactions (see e.g. [19]) may explore particle-unstable resonances in $\Lambda\Lambda$ -hypernuclei. Combining these three different methods we will have access to the complete level scheme of $\Lambda\Lambda$ -hypernuclei.

Complemented by hyperon-hyperon correlation studies in heavy ion collisions, these measurements will provide comprehensive information on the hyperon-hyperon interaction and on the role of $\Lambda\Lambda - \Sigma\Sigma - \Xi N$ mixing in nuclei [20].

2. High resolution γ -spectroscopy of $\Lambda\Lambda$ -hypernuclei at FAIR

Since the first ideas of an antiproton storage ring HESR at the international Facility for Antiproton and Ion Research (FAIR), the high resolution γ -spectroscopy of $\Lambda\Lambda$ -hypernuclei is part of the core programme of the PANDA experiment [12, 21, 22]. To produce $\Lambda\Lambda$ -hypernuclei in a ‘controlled’ way the conversion of a captured Ξ^- and a proton into two Λ particles can be used (see right part of Fig. 1). The essential ingredient for the hypernuclear and hyperatom studies planned at PANDA is therefore the production of slow Ξ^- which can be stopped prior to their decay in a secondary target, eventually leading to the formation of bound hyperonic systems. Combined with large cross sections for the production of associated hyperon-antihyperon pairs, antiprotons circulating in a storage ring are ideally suited for exploring strange baryonic systems. Low momentum Ξ^- can be produced via the $\bar{p}p \rightarrow \Xi^- \bar{\Xi}^+$ or $\bar{p}n \rightarrow \Xi^- \bar{\Xi}^0$ reactions within a complex nucleus where the produced Ξ^- can re-scatter [12]. The advantage as compared to the kaon induced Ξ production is that antiprotons are stable and can be retained in a storage ring thus allowing rather high luminosities. Reactions close to the $\Xi\bar{\Xi}$ threshold also minimize the production of associated particles as well as the number of secondary particles produced in other nuclear reactions.

In addition to the general purpose PANDA setup [22], the hypernuclear experiment requires a dedicated primary target to produce low momentum Ξ^- , an active secondary target of silicon layers and a suitable amount of absorber material to stop the Ξ^- hyperons and to detect pions from the weak decay of $\Lambda\Lambda$ - and Λ -hypernuclei and a high purity germanium (HPGe) array as γ -detectors. The design of the hypernucleus setup is approaching its final stage and the construction of the required detector components has started (see below). In the following we will present some details concerning the choice of the primary target as an example of these studies.

The main task of the primary target is the production of Ξ^- hyperons which can be slowed down and finally stopped in the secondary target material prior to their decay. The stopping probability depends on the detailed geometry of the target setup. In order to identify the optimal target material we performed a set of simulations with the Giessen Boltzmann-Uehling-Uhlenbeck transport model (GiBUU, Release 1.5) [23] followed by full GEANT4 simulations

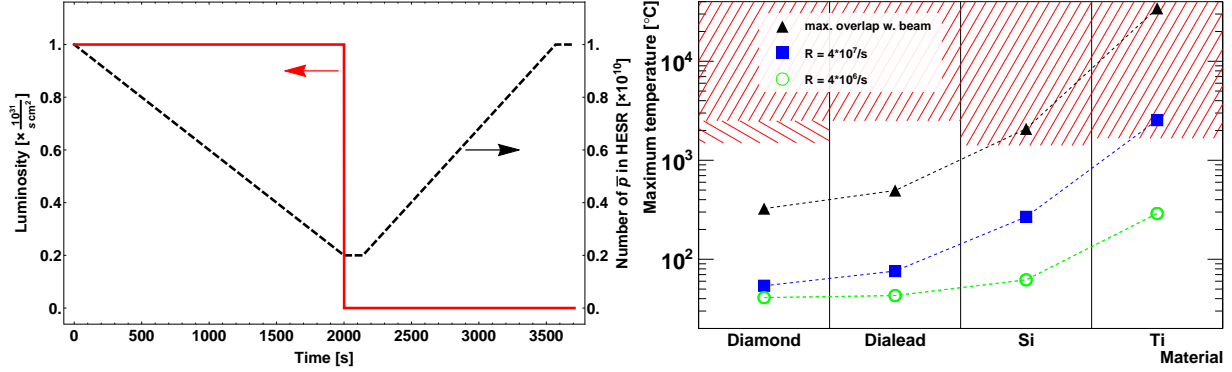


Figure 3. Left: Number of antiprotons circulating in the HESR during a cycle. The constant luminosity over a period of 2000 s is achieved by moving the carbon fiber with a radius of 5 μm from a initial displacement of 3 mm to about 2.5 mm towards the beam axis. Right: Maximum temperature reached in the primary target filaments for different materials and an interaction rate during the measurement periods of $4 \cdot 10^6 \text{s}^{-1}$ (dots) and $4 \cdot 10^7 \text{s}^{-1}$ (squares). The triangles show the temperature at maximum overlap if the beam accidentally crosses the target filament. For all filaments a radius of 5 μm was assumed. The red shaded region indicates the melting limit.

Target-material	Ξ^- production probability	Ξ^- stopping probability	luminosity loss factor	FoM
^{12}C	$(2.22 \pm 0.02) \cdot 10^{-5}$	$(3.24 \pm 0.04) \cdot 10^{-3}$	0.539	$(3.87 \pm 0.06) \cdot 10^{-8}$
^{28}Si	$(2.42 \pm 0.04) \cdot 10^{-5}$	$(3.41 \pm 0.07) \cdot 10^{-3}$	0.339	$(2.80 \pm 0.08) \cdot 10^{-8}$
^{48}Ti	$(2.48 \pm 0.04) \cdot 10^{-5}$	$(3.79 \pm 0.07) \cdot 10^{-3}$	0.245	$(2.31 \pm 0.05) \cdot 10^{-8}$

Table 1. Ξ^- production probability with respect to all inclusive interactions predicted by GiBUU transport calculations and stopping probability within the secondary boron absorbers for all produced Ξ^- for primary targets made of ^{12}C , ^{28}Si , and ^{48}Ti . The fourth column gives the luminosity decrease caused by Coulomb scattering and energy straggling [24]. As a figure-of-merit (FoM) the product of these three numbers is given in the last column.

[25] taking into account all details of the secondary target geometry. Because of the finite lifetime of hyperons only Ξ^- 's with momenta below 500 MeV/c have a sizable chance to be stopped prior to their decay. The Ξ^- production with respect all nuclear interactions in heavy targets shows only a slight enhancement, somewhat less than in previous preliminary cascade calculations [26] (Fig. 2, left). However, heavier targets cause substantial beam heating mainly by Coulomb scattering and energy straggling [24]. Tab. 1 presents the Ξ^- production probability with respect to all inclusive interactions predicted by GiBUU transport calculations and their stopping probability for primary targets made of ^{12}C , ^{28}Si , and ^{48}Ti . The fourth column gives the luminosity decrease caused by Coulomb scattering and energy straggling in the HESR [24]. As a figure-of-merit (FoM) the product of these three numbers is given in the last column. As can be seen from this table, a light carbon target is clearly preferable.

In addition, there are several other points which need to be considered and which also favour carbon as a primary

Target-material	Thermal conductivity [W/mK]	Tensile modulus [GPa]	density [g/cm ³]	melting/transition temperature [°C]
CVD Diamond	1800-2500	1050-1210	3.52	3500 [1500]
DIALEAD TM fiber [27]	800	935	2.20	2500
^{28}Si	149	130-185	2.33	1414
^{48}Ti	22	110	4.51	1668
<i>nat</i> Cu	401	120	8.96	1538

Table 2. Physical properties of possible target materials. As reference the numbers for copper are also given. Note, that the graphitization of diamond takes place already at lower temperature around 1500 °C. The DIALEADTM carbon fiber is produced at temperature around 3000 °C and gets malleable around 2500 °C [27].

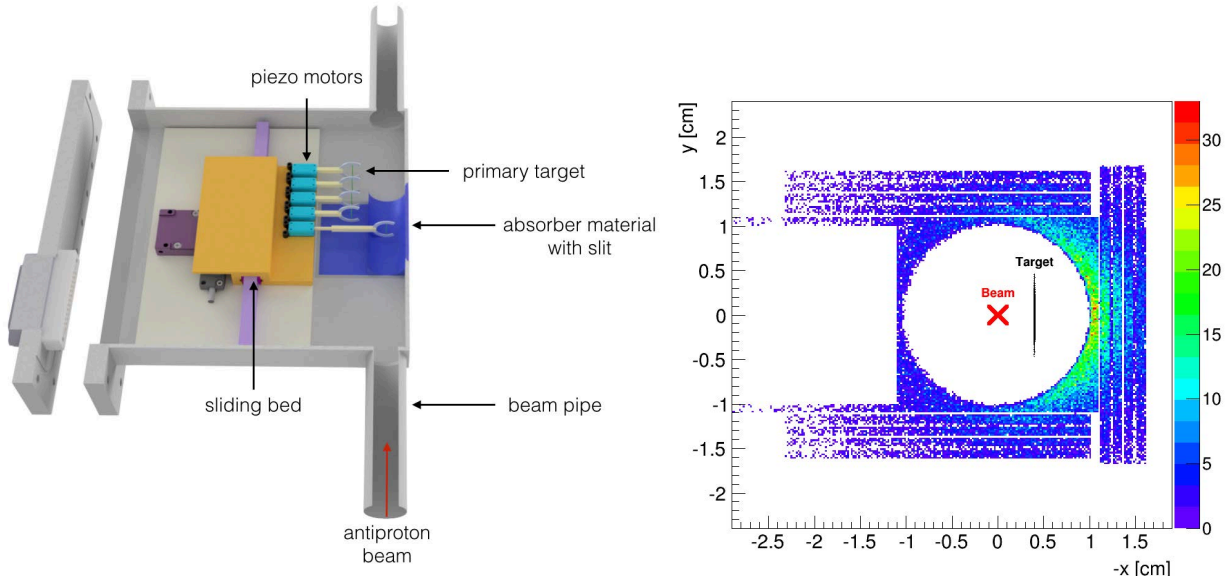


Figure 4. Left: CAD drawing of the primary target setup. Right: Distribution of the Ξ^- stopping points in layers of the secondary target material in a plane transverse to the beam direction. The empty bands mark the location of the silicon strip detectors. Because of the finite lifetime of Ξ^- , a minimal distance between the primary target and the absorber material is essential to reach the optimal stopping probability.

77 target material. The primary target consists of a thin filament which will be operated in the halo of the antiproton
 78 beam. The continuous decrease of the number of antiprotons circulating in the HESR will be compensated by moving
 79 the target filament closer to the beam axis. A similar scheme was already developed by the EDDA collaboration at
 80 COSY [28]. The left part of Fig. 3 shows a possible HESR cycle during the startup phase of PANDA. In this phase
 81 the antiproton collector ring RESR will not be available and the maximum number of antiprotons circulating in the
 82 HESR is therefore limited to 10^{10} . Furthermore, the minimal expected \bar{p} production rate is $5.6 \cdot 10^6 \text{ s}^{-1}$. Such a scenario
 83 allows an average interaction rate over the full cycle of at least $2.2 \cdot 10^6 \text{ s}^{-1}$ in case of a target fiber with a radius of
 84 $5 \mu\text{m}$. The constant luminosity during the measurement period of 2000 s is achieved by moving the carbon filament
 85 from a distance of 3 mm down to about 2.5 mm from the beam center. Since at present the detailed shape of the beam
 86 profile is not known, we assumed a gaussian distribution with a width of $\sigma=1 \text{ mm}$. At PANDA the rate measured by
 87 the luminosity monitor will be used to control the interaction rate independently of the exact distribution of the beam
 88 profile.

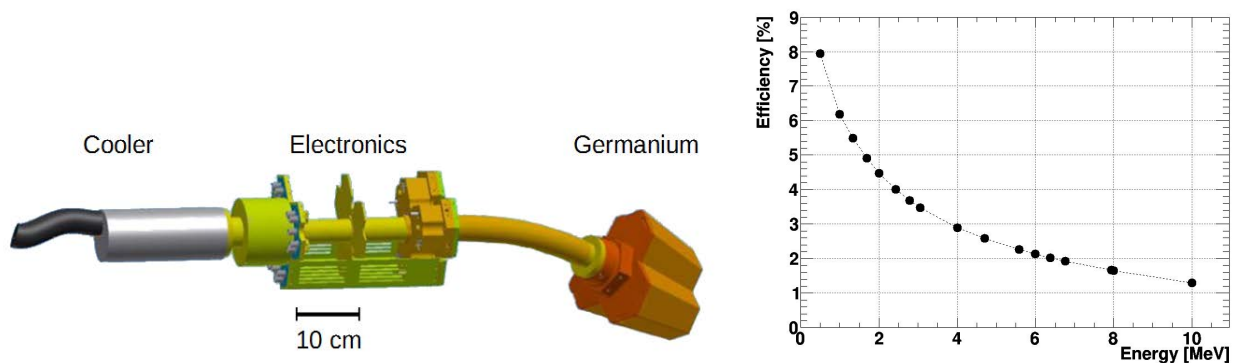


Figure 5. Left: Final design of one of the triple PANDA Germanium Assembly PANGEA. Right: Expected full energy-peak efficiency of the PANGEA setup in PANDA.

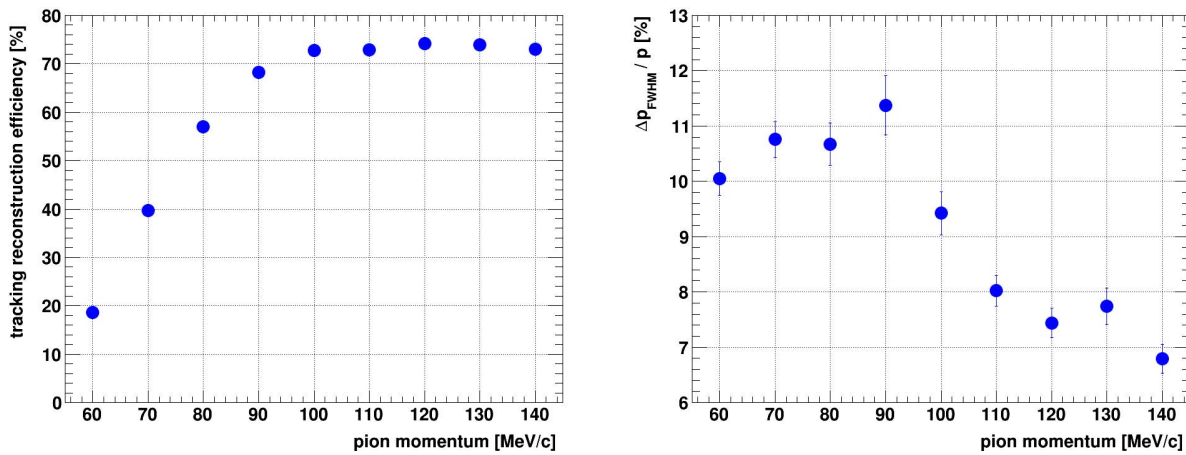


Figure 6. Left: Reconstruction efficiency of negative pions emitted isotropically from hypernuclei produced in the absorbers of the secondary target. Right: Relative momentum resolution of reconstructed weak decay pions as function of their momentum.

89 Replacing the internal target during operation is difficult in a storage ring experiment. Therefore, the thermal and
 90 mechanical stabilities of the target are important issues for a safe operation over several months. Besides diamond,
 91 silicon and titanium we also consider a carbon nanofiber [27] as potential target. All these materials show high
 92 melting temperatures and good electric conductivity (see Tab. 2). For comparison the properties of copper are also
 93 listed. At $4 \cdot 10^6$ interactions per second more than $50 \mu\text{W}$ will be deposited in the target filament by the energy loss of
 94 antiprotons passing the target. Heat transport calculations, assuming a gaussian distributed beam with $\sigma=1$ mm and
 95 target radii of $5 \mu\text{m}$ resulted in maximum temperatures indicated by the open circles in the right part of Fig. 3.

96 For all four target materials this temperature is below the melting temperature indicated by the red shaded region
 97 in Fig. 3. However, increasing the beam intensity by a factor of 10, the titanium target is likely to be destroyed. The
 98 same happens to a silicon strip target if the full beam crosses the target accidentally. On the other hand, a diamond or
 99 carbon fiber target can be safely operated even at the highest interaction rate expected at PANDA (see blue squares in
 100 Fig. 3).

101 Particle background is another important issue. The right part of Fig. 2 shows the produced charged particles
 102 within the angular range covered by the silicon detectors of the secondary target (blue circles) and neutrons in the ac-
 103 ceptance of the Germanium array (red triangles) normalized to the number of Ξ^- with momenta less than $500 \text{ MeV}/c$.
 104 Because of the more backward oriented particle distributions for heavier target nuclei, the background situation also
 105 favors a light target material.

106 Because of the short lifetime of the Ξ^- hyperons and their brief stopping time in the secondary target, it is essential
 107 to place the secondary absorber as close as possible to the primary target to reach a maximum stopping probability.
 108 Since the distance between the antiproton beam and the wall of the vacuum chamber must not go below a limit of
 109 10 mm, the usage of a thin vacuum window (areal density $\approx 100 \text{ mg}/\text{cm}^2$) would require an additional offset of 1-2 mm
 110 due to the inward bending of the window foil. In order to avoid such a foil we have decided to build the wall of the
 111 vacuum chamber in the region of the secondary target out of 1 mm thick secondary absorber material. Additional
 112 absorber material will be placed inside the vacuum chamber in the edges, thus forming a cylindrical beam pipe (see
 113 Fig. 4). Beryllium, boron, boron carbide or diamond are possible window materials. In the following we show results
 114 for boron absorbers. The distribution of the Ξ^- stopping points shown in Fig. 4 illustrates the necessity to place the
 115 absorber material as close as possible to the beam axis.

116 The $\Lambda\Lambda$ -hypersystems produced at PANDA after the Ξ^- conversion into to Λ hyperons, are usually highly excited
 117 and may fragment [21]. Sometimes particle bound $\Lambda\Lambda$ -hypernuclei will be produced. Those in excited states will
 118 decay via γ -emission which will be detected in an germanium detector system placed at backward angles. For the
 119 PANDA Germanium array, 48 EUROBALL detectors need to be reconfigured into triple units. The PANGEA (PANda
 120 Germanium Array) triple cluster is a cooperative project between GSI Darmstadt and the Helmholtz Institute Mainz

121 for the $\bar{\text{P}}\text{ANDA}$ collaboration (see left part in Fig. 5). The unique feature of the PANGEA cryostat is its minimal
 122 cross section actually defined by the footprint of the triple crystal arrangement, and the use of an electrical cooling
 123 engine (X-Cooler II, III from MMR, respectively Ametec). At the Super-FRS the same components will be used
 124 by the DEGAS (DESPEC Germanium Array Spectrometer) detectors [29]. The only mechanical difference is that
 125 the PANGEA triple cryostat has a flexible neck between the cooling engine and the detector head. Reconfiguring
 126 PANGEA into DEGAS this flexible neck will be replaced by a simple rigid tube. The PANGEA triple cryostat
 127 comprises on board preamplifiers, high voltage (HV) modules, a bias shut down (BSD) modul, a power supply module
 128 generating all the voltage needed from 48V supply, ADC modules based on nanoMCA-module (LabZY) and a control
 129 module based on a micro controller. The PANGEA triple clusters will be arranged at backward angles. The right part
 130 of Fig. 5 shows the expected efficiency of this setup in $\bar{\text{P}}\text{ANDA}$.

131 Light $\Lambda\Lambda$ -hypernuclei in the mass region below $A \approx 12$ which have reached their ground state will decay weakly
 132 emitting eventually one or two negative pions (see Fig. 1). The momenta of these pions are expected to cover a range
 133 from about 70 to 140 MeV/c [18, 30]. The left part of Fig. 6 shows the reconstruction efficiency of pions in this
 134 momentum range emitted isotropically from the Ξ^- stopping points displayed in the right part of Fig. 4. Because of
 135 the compact geometry of the secondary target, efficiencies larger than 70% can be achieved. The momenta of these
 136 pions can be reconstructed with a relative precision (FWHM) of better than 11% (see right part of Fig. 6). This good
 137 reconstruction capability of the secondary target allows to use these low momentum pions as a selection criterion for
 138 hypernucleus production and will help to reduce background events. According to the GiBUU simulations for about
 139 half of the produced Ξ^- in $\bar{\text{p}}^{12}\text{C}$ reactions a Ξ^0 ($\approx 30\%$) or a Ξ^+ ($\approx 18\%$) escapes the ^{12}C target nucleus. These Ξ decay
 140 with nearly 100% into an $\Lambda\pi$ which will be used as an additional, rather exclusive trigger.

141 Not all steps shown in the scheme in the right part of Fig. 1 can be treated by GEANT simulations as e.g. the
 142 atomic cascade. They require independent theoretical input. The final rate estimate takes the Ξ^- production and
 143 stopping probability (Tab. 1) as well as the capture, conversion and fragmentation processes (see e.g. [21, 31–34])
 144 into account. In our approach we take the *excited* $\Lambda\Lambda$ pre-fragment formed after the $\Xi^- \text{p} \rightarrow \Lambda\Lambda$ conversion as a
 145 starting point [21]. At an average antiproton interaction rate of $5 \cdot 10^6 \text{ s}^{-1}$ and with the present design, $\bar{\text{P}}\text{ANDA}$ will
 146 produce approximately $3.3 \cdot 10^4$ Ξ^- 's per day stopped within the boron absorber of the secondary target. Triggering
 147 on the detection of two successive weak pionic [35] decays or the $\bar{\Lambda}$ detected within the $\bar{\text{P}}\text{ANDA}$ setup and with the
 148 full energy γ -efficiency (Fig. 5) we expect approximately 10 detected γ -transitions per month for several $\Lambda\Lambda$ -nuclei
 149 produced in the fragmentation process after the $\text{p}\Xi^- \rightarrow \Lambda\Lambda$ conversion (see e.g. [21]). A major task for the future is
 150 to develop by means of the GiBUU events a strategy to further suppress inclusive low momentum pion events. The
 151 topology of the pion tracks (e.g. closed distance of approach with respect to the target filament) and the associated
 152 particles measured within the $\bar{\text{P}}\text{ANDA}$ detector are presently being studied.

153 3. Hyperatoms at $\bar{\text{P}}\text{ANDA}$

154 A well understood detection system and high luminosities will be mandatory for the study of $\Lambda\Lambda$ -hypernuclei at
 155 $\bar{\text{P}}\text{ANDA}$. During the initial operation of the hypernuclear setup we therefore plan to study Ξ^- -atoms [12, 36] (see also
 156 right part of Fig. 1). At the same time such a measurement will allow to develop and to test the hypernuclear setup of
 157 $\bar{\text{P}}\text{ANDA}$ under real running conditions.

158 In line with the $\Lambda\Lambda$ -hypernucleus study, a close proximity between the primary target and the secondary absorber
 159 is mandatory. In this case absorbers can be heavy elements like Fe or Ta. As before, the vacuum chamber can be built
 160 from this absorber material, thus optimizing the hyperon stopping probability. At the same time the geometry of the
 161 secondary absorber should minimize the absorption of the atomic X-rays. A first preliminary design of the secondary
 162 absorber is shown in the left part of Fig. 7. The shape of the rim is optimized for maximum Ξ^- stopping at minimal
 163 losses of γ 's emitted from the hyperatoms. The distribution of the Ξ^- stopping points are shown in the right part of
 164 Fig. 7. Even at an antiproton interaction rate of $2 \cdot 10^6 \text{ s}^{-1}$ $\bar{\text{P}}\text{ANDA}$ will be able to produce approximately $6 \cdot 10^5$ stopped
 165 Ξ^- hyperons per month in these heavy targets which is comparable to the maximum rate expected at J-PARC of about
 166 $7 \cdot 10^5$ stopped Ξ^- per month [37]. Since only very little information on Ξ^- production in antiproton-nucleus collisions
 167 is presently available, it is clear that the design of the secondary absorber should be finalized once better experimental
 168 information on the angular and momentum distributions of Ξ^- will be available.

169 The study of Ξ^- -atoms will also serve as an initial step towards a study of Ω^- -atoms. Like all composite particles
 170 baryons are expected to be deformed objects. However, for spin $J=0$ and $1/2$ hadrons, the spectroscopic quadrupole

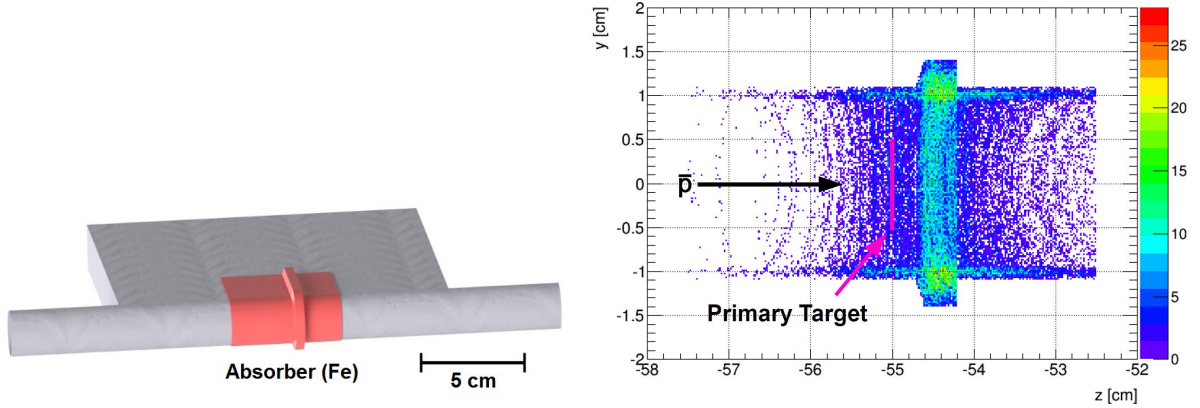


Figure 7. Left: Schematic drawing of the secondary target chamber for the hyperatom study at PANDA. The beam enters from left. Right: Stopping points predicted by full GEANT simulations which are based on GiBUU events. The shape of the rim is optimized for maximum Ξ^- stopping and minimal losses of γ 's emitted from the hyperatoms.

171 moment Q vanishes even though the intrinsic quadrupole moment Q_0 may be finite. On the other hand, for spin-3/2
 172 particles the intrinsic quadrupole moment can be deduced from the spectroscopic moment according to (see e.g. [38])

$$Q = \frac{J(2J-1)}{(J+1)(2J+3)} Q_0. \quad (1)$$

173 The long lifetime and its spin 3/2 makes the Ω^- the only candidate to obtain direct experimental information on the
 174 shape of an individual baryon. This measurement would be an important complement to the world wide activities
 175 trying to nail down the shape of the proton or the transition quadrupole moment of baryons.

Model	Q_Ω [$e \cdot \text{fm}^2$]	Ref.
NRQM	0.02	[39]
NRQM	0.004	[40]
NRQM	0.031	[41]
SU(3) Bag model	0.052	[42]
NRQM with mesons	0.0057	[43]
NQM	0.028	[44]
Lattice QCD	0.004 ± 0.005	[45]
HB χ PT	0.009 ± 0.005	[46]
Skyrme	0.024	[47]
Skyrme	0.0	[48]
QM	0.022	[49]
χ QM	0.026	[50]
GP QCD	0.024	[51]
Lattice QCD	0.0086 ± 0.0012	[52]
QCD-SR	0.1 ± 0.03	[53]
χ PT+qQCD	0.0086	[54]
Lattice QCD	0.0118 ± 0.0012	[55, 56]
RQM+Lattice QCD	0.0096 ± 0.0002	[56]

Table 3. Predictions for the quadrupole moment of the Ω^- baryon.

176 Measuring the quadrupole moment of the Ω^- , or setting a limit to its value, would provide very useful constraints
 177 on the composite models of baryons (see Tab. 3). Unlike in the case of the nucleon, pion exchange is not relevant
 178 and the role of heavier mesons is strongly suppressed. Therefore, meson cloud corrections to the valence quark core

are expected to be small [56]. Because contributions from light quarks are small, the quadrupole moment of the Ω^- will also be a sensitive benchmark test for lattice QCD simulations. For negatively charged baryons like the Ω^- , a positive (negative) quadrupole form factor would signal an oblate (prolate) distribution of the three s -quarks. All recent calculations predict an intrinsic quadrupole moment Q_Ω of the order of $0.01 e\text{-fm}^2$ (see Tab. 3).

It is important to note that the deformation of the Ω^- baryon is only one aspect of Ω^- -hyperatoms addressed at PANDA. Similar to the case of Ξ^- -atoms, the shift and broadening of transitions between orbits close to the nucleus provide a complementary tool for studying strong interactions and nuclear medium effects [57, 58]. Thus, Ω^- -hyperatoms represent a unique chance to explore the interaction of $|S|=3$ baryons in a nuclear system.

Indeed, it was suggested by Alvarez [59] that three emulsion events observed in 1954 [60, 61] can be interpreted as Ω^- decays (10 years prior to its discovery at Brookhaven [62]). Out of these 3 events, two can be attributed to the decay of atomically bound Ω^- . This observation suggests that the formation of Ω^- -atoms is possible and may not be unusual once a Ω^- hyperon has been slowed down. Unfortunately, not even the elementary production cross section for $\Omega^- \bar{\Omega}^+$ pairs in antiproton-proton collisions is experimentally known and even predictions are scarce [63] and may have large uncertainties. Therefore, quantitative predictions for the yield of atomic transitions in Ω^- -atoms are not possible at the moment. Nevertheless, although the present considerations indicate that the study of Ω^- -atoms will not be a day-1 experiment at PANDA, this discussion also shows that such a measurement is within reach. Of course, like in the case of $\Lambda\Lambda$ -hypernuclei, a well understood detection system and high luminosities will be mandatory for this measurement.

4. Anticascades in Nuclei

The interaction of antibaryons in nuclei provides a unique opportunity to elucidate strong in-medium effects in baryonic systems. Unfortunately, antihyperons annihilate quickly in nuclei and conventional spectroscopic studies of bound systems are not feasible. Complementing the information on Ξ^- from hyperatoms, quantitative information on the antihyperon potentials may be obtained via exclusive antihyperon-hyperon pair production close to threshold in antiproton-nucleus interactions [64–66]. The preliminary calculations of Ref. [64, 65] revealed significant sensitivities of the transverse momentum asymmetry α_T which is defined in terms of the transverse momenta of the coincident particles

$$\alpha_T = \frac{p_T(Y) - p_T(\bar{Y})}{p_T(Y) + p_T(\bar{Y})} \quad (2)$$

to the depth of the antihyperon potential. In order to go beyond the simplified calculations presented in Refs. [64, 65] and to include simultaneously secondary deflection and absorption effects, we recently performed [66] more realistic calculations of this new observable with the Giessen Boltzmann-Uehling-Uhlenbeck transport model (GiBUU, Release 1.5) [23] for $\Lambda\bar{\Lambda}$ pairs. Here we present first results for $\Xi^+ \Xi^-$ pairs produced in $\bar{p}+^{12}\text{C}$ interactions at 2.9 GeV/c.

Fig. 8 shows the GiBUU prediction for the average transverse asymmetry α_T (Eq. 2) plotted as a function of the longitudinal momentum asymmetry α_L which is defined for each event as

$$\alpha_L = \frac{p_L(Y) - p_L(\bar{Y})}{p_L(Y) + p_L(\bar{Y})}. \quad (3)$$

As for $\Lambda\bar{\Lambda}$ pairs [66], the $\Sigma^-\bar{\Lambda}$ pairs (left) show a remarkable sensitivity of α_T on the scaling factor $\xi_{\bar{\Lambda}}$ of the $\bar{\Lambda}$ -potential [66]. In the GiBUU code non-linear derivative interactions are not yet included and a simple scaling factor $\xi_{\bar{p}} = 0.22$ was already previously applied for the antiproton potential to ensure a Schrödinger equivalent antiproton potential of about 150 MeV at saturation density [67]. No experimental information exists so far for antihyperons in nuclei and G-parity symmetry is therefore usually adopted to specify their default potentials. While this corresponds to $\xi_{\bar{\Lambda}} = 1$, a value of $\xi_{\bar{\Lambda}} \approx 0.2$ might be a more appropriate considering antiproton data. In Ref. [66] it was demonstrated that the sensitivity of α_T to the scaling factor $\xi_{\bar{\Lambda}}$ is strongly related to re-scattering processes of the hyperons and antihyperons within the target nucleus. For positive values of α_L where the $\bar{\Lambda}$ is emitted backward with respect to the hyperon, the statistics is too low to draw quantitative conclusions in the present simulation.

In the right part of Fig. 8 we show the first attempt to calculate the momentum asymmetry for $\Xi^-\bar{\Xi}^+$ -pair production in 2.9 GeV/c \bar{p} - ^{12}C interactions. In these GiBUU calculations about 79 million inclusive events were generated for

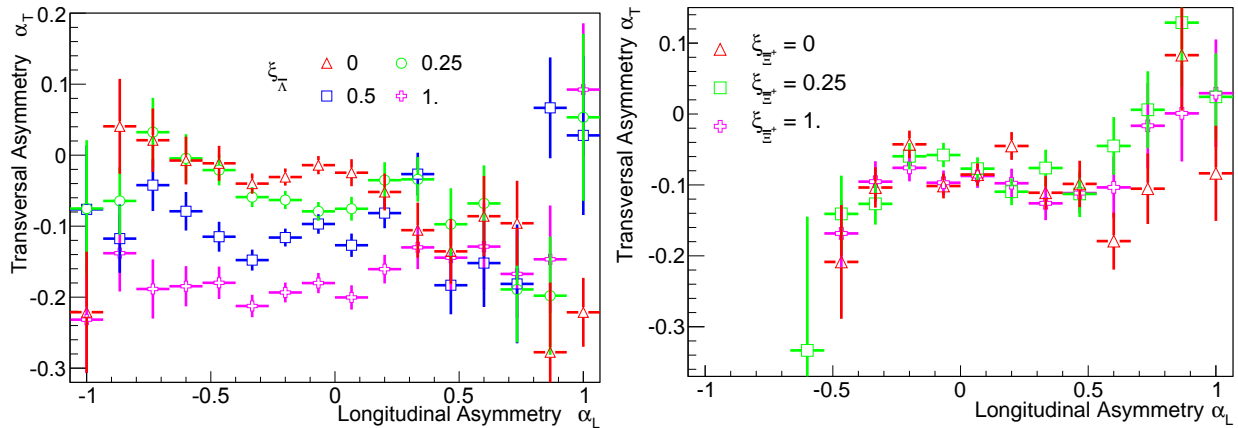


Figure 8. Average transverse momentum asymmetry as a function of the longitudinal momentum asymmetry for $\Sigma^-\bar{\Lambda}$ pairs (left) and $\Xi^-\bar{\Xi}^+$ pairs (right) produced exclusively in 1.696 GeV/c \bar{p} - ^{20}Ne and 2.9 GeV/c \bar{p} - ^{12}C interactions, respectively. The different symbols show the GiBUU predictions for different scaling factors for the antihyperon potentials.

each scaling factor $\xi_{\Xi^+}^{\bar{\Xi}^+}$ of the $\bar{\Xi}^+$ potential. In addition, the production of hyperon-antihyperon pairs was artificially enhanced by a factor of 10 [66]. Thus, the present statistics corresponds to 790 million inclusive reactions. For an average antiproton interaction rate of $2 \cdot 10^6 \text{ s}^{-1}$ this would reflect a running time of about 6 minutes. For each value of the scaling factor $\xi_{\Xi^+}^{\bar{\Xi}^+}$, about 1800 $\Xi^-\bar{\Xi}^+$ pairs were found. Obviously even this large amount of produced events does not allow to determine the sensitivity of the simulations to the anticascade potential. At least a factor of 10 more events will be needed to draw quantitative conclusions on the $\bar{\Xi}^+$ -potential. However, what the present calculations already show is that the variation of the transverse asymmetry for $0 \leq \xi_{\Xi^+}^{\bar{\Xi}^+} \leq 1$ does not exceed a value of 0.1. This is consistent with the calculations presented in Refs. [64, 65].

Assuming a pair reconstruction probability of 10% (1%), PANDA may detect about 30 (3) $\Xi^-\bar{\Xi}^+$ pairs per minute. The accumulation of 10^5 $\Xi^-\bar{\Xi}^+$ pairs will then require a running time of about 2 day (23 days). Such periods are compatible with the earlier estimates based on a schematic model [64, 65]. Thus this measurement can easily be performed at PANDA once a reasonable interaction rate for nuclear targets has been established.

To summarize, stored antiprotons beams in the GeV range represent a unparalleled factory for hyperon-antihyperon pairs. Their outstanding large production probability in antiproton collisions will open the floodgates for a series of new studies of strange hadronic systems with unprecedented precision. Several of these unique experiments are possible at reduced luminosities in the commissioning phase of PANDA, like the study of antihyperons in nuclear systems and the spectroscopy of multistrange Ξ -atoms. The high resolution γ -spectroscopy of $\Lambda\Lambda$ -hypernuclei will require an interaction rate in the region of $5 \cdot 10^6 \text{ s}^{-1}$. The spectroscopy of Ω^- -atoms will be challenging, but seems possible.

5. Acknowledgements

The success of this work relies critically on the expertise and dedication of the computing organizations that support PANDA. We acknowledge financial support from the Science and Technology Facilities Council (STFC), British funding agency, Great Britain; the Bhabha Atomic Research Center (BARC) and the Indian Institute of Technology, Mumbai, India; the Bundesministerium für Bildung und Forschung (BMBF), Germany; the Carl-Zeiss-Stiftung 21-0563-2.8/122/1 and 21-0563-2.8/131/1, Mainz, Germany; the Center for Advanced Radiation Technology (KVI-CART), Groningen, Netherland; the CNRS/IN2P3 and the Université Paris-Sud, France; the Deutsche Forschungsgemeinschaft (DFG), Germany; the Deutscher Akademischer Austauschdienst (DAAD), Germany; the Forschungszentrum Jülich GmbH, Jülich, Germany; the FP7 HP3 GA283286, European Commission funding; the Gesellschaft für Schwerionenforschung GmbH (GSI), Darmstadt, Germany; the Helmholtz-Gemeinschaft Deutscher Forschungszentren (HGF), Germany; the INTAS, European Commission funding; the Institute of High Energy Physics (IHEP) and the Chinese Academy of Sciences, Beijing, China; the Istituto Nazionale di Fisica Nucleare (INFN), Italy;

the Ministerio de Educacion y Ciencia (MEC) under grant FPA2006-12120-C03-02; the Polish Ministry of Science and Higher Education (MNiSW) grant No. 2593/7, PR UE/2012/2, and the National Science Center (NCN) DEC-2013/09/N/ST2/02180, Poland; the State Atomic Energy Corporation Rosatom, National Research Center Kurchatov Institute, Russia; the Schweizerischer Nationalfonds zur Forderung der wissenschaftlichen Forschung (SNF), Swiss; the Stefan Meyer Institut für Subatomare Physik and the Österreichische Akademie der Wissenschaften, Wien, Austria; the Swedish Research Council, Sweden.

- [1] B.P. Abbott *et al.*, Phys. Rev. Lett. **116**, 061102 (2016).
- [2] D. Psaltis, Living Rev. Relativity, **11**, 9 (2008).
- [3] P.B. Demorest *et al.*, Nature **467**, 1081 (2010).
- [4] J. Antoniadis *et al.*, Science **340**, 1233232 (2013).
- [5] S. DeDeo, D. Psaltis, Phys. Rev. Lett. **90**, 141101 (2003).
- [6] S. Capozziello, M. De Laurentis, R. Farinelli, and S.D. Odintsov, Phys. Rev. D **93**, 023501 (2016).
- [7] A.V. Astashenok, S. Capozziello, and S.D. Odintsov, Phys. Rev. D **89**, 103509 (2014).
- [8] A. Esser *et al.*, Phys. Rev. Lett. **114**, 232501 (2015).
- [9] T.O. Yamamoto *et al.*, Phys. Rev. Lett. **115**, 222501 (2015).
- [10] D. Gazda, A. Gal, Phys. Rev. Lett. **116**, 122501 (2016).
- [11] K. Nakazawa for KEK-E176, E373 and J-PARC E07 collaborators, Nucl. Phys. A **835**, 207 (2010).
- [12] J. Pochodzalla, Nucl. Instr. Meth B **214**, 149 (2004).
- [13] A.S. Botvina and J. Pochodzalla, Phys. Rev. C **76**, 024909 (2007).
- [14] A.S. Botvina, K.K. Gudima and J. Pochodzalla, Phys. Rev. C **88**, 054605 (2013).
- [15] A.S. Botvina, J. Steinheimer, E. Bratkovskaya, M. Bleicher, J. Pochodzalla, Phys. Lett. B **742**, 7 (2015).
- [16] B.I. Abelev *et al.*, (STAR Collaboration), Science **328**, 58 (2010), DOI: 10.1126/science.1183980.
- [17] J. Adam *et al.*, (ALICE Collaboration), Phys. Lett. B **754**, 360 (2016).
- [18] J. K. Ahn *et al.*, Phys. Rev. Lett. **87**, 132504 (2001).
- [19] J. Pochodzalla *et al.*, Phys. Rev. C **35**, 1695 (1987).
- [20] see e.g. E. Hiyama, T. Yamada, Progress in Particle and Nuclear Physics **63**, 339 (2009) and references therein.
- [21] A. Sanchez Lorente, A.S. Botvina, and J. Pochodzalla, Phys. Lett. B **697**, 222 (2011).
- [22] PANDA Collaboration: Physics Performance Report for PANDA: Strong Interaction Studies with Antiprotons, arXiv:0903.3905 [hep-ex]
- [23] O. Buss, T. Gaitanos, K. Gallmeister, H. van Hees, M. Kaskulov, O. Lalakulich, A.B. Larionov, T. Leitner, J. Weil, U. Mosel, Phys. Rep. **512**, 1 (2012).
- [24] A. Lehrach, O. Boine-Frankenheim, F. Hinterberger, R. Maier, D. Prasuhn, Nucl. Instr. Meth. in Phys. Res. A **561**, 289 (2006).
- [25] GEANT4 Collaboration, Nucl. Instr. Meth A **506**, 250 (2003).
- [26] F. Ferro, M. Agnello, F. Iazzi, K. Szymańska, Nucl. Phys. A **789**, 209 (2007).
- [27] Mitsubishi Rayon Co., LTD, <https://www.mrc.co.jp/dialead/english/dialed.html> (2015).
- [28] The EDDA Collaboration, D. Albers *et al.*, Eur. Phys. J. A **22**, 125 (2004).
- [29] Technical Report for the Design, Construction and Commissioning of the DESPEC Germanium Array Spectrometer - DEGAS; ed. B. Cederwall, M. Doncel, A. Gadea, J. Gerl, I. Kojouharov, R. Palit; (2014) http://www.fair-center.de/fileadmin/fair/experiments/NUSTAR/Pdf/TDRs/TDR_HISPEC_DESPEC_DEGAS_public.pdf
- [30] FINUDA Collaboration, M. Agnello *et al.*, Phys. Lett. B **618**, 139 (2009).
- [31] M. Sano, M. Wakai, Y. Yamamoto, Prog. Theor. Phys. **87**, 957 (1992).
- [32] K. Ikeda, T. Fukuda, T. Motoba, M. Takahashi and Y. Yamamoto, Prog. Theor. Phys. **91**, 747 (1994).
- [33] T. Yamada and K. Ikeda, Phys. Rev. C **56**, 3216 (1997).
- [34] Y. Hirata, Y. Nara, A. Ohnishi, T. Harada, J. Randrup, Prog. Theor. Phys. **102**, 89 (1999).
- [35] A. Sanchez Lorente, Hyperfine Interact **213**, 41 (2012).
- [36] F. Iazzi and K. Szymanska, Hyperfine Interactions **193**, 89 (2009)
- [37] K. Tanida (spokesperson) *et al.*, J-PARC P03 proposal, http://j-parc.jp/researcher/Hadron/en/Proposal_e.html.
- [38] A. Messiah, *Quantum Mechanics II* (North-Holland Publishing, Amsterdam, 1965).
- [39] S.S. Gershtein, Yu.M. Zioviev, Sov. J. Nucl. Phys. **33**, 772 (1981).
- [40] J.-M. Richard, Z. Phys. C **12**, 369 (1982).
- [41] N. Isgur, G. Karl, R. Koniuk, Phys. Rev. D **25**, 2395 (1982).
- [42] M.I. Krivoruchenko, Sov. J. Nucl. Phys. **45**, 109 (1987).
- [43] W.J. Leonard, W.J. Gerace, Phys. Rev. D **41**, 924 (1990).
- [44] M.I. Krivoruchenko, M.M. Giannini, Phys. Rev. D **43**, 3763 (1991).
- [45] D.B. Leinweber, T. Draper, R.M. Woloshyn, Phys. Rev. D. **46**, 3067 (1992).
- [46] M.N. Butler, M.J. Savage, R.P. Springer, Phys. Rev. D **49**, 3459 (1994).
- [47] J. Kroll, B. Schwesinger, Phys. Lett. B **334**, 287 (1994).
- [48] Y. Oh, Mod. Phys. Lett.A **10**, 1027(1995).
- [49] A.J. Buchmann, Z. Naturforschung **52a**, 877 (1997).
- [50] G. Wagner, A.J. Buchmann, A. Fässler, J. Phys. G **26**, 267 (2000).
- [51] A.J. Buchmann, E.M. Henley, Phys. Rev. D **65**, 073017 (2002).
- [52] S. Boinepalli, D. B. Leinweber, P. J. Moran, A. G. Williams, J. M. Zanotti, and J. B. Zhang, Phys. Rev. D **80**, 054505 (2009).
- [53] K. Azizi, Eur. Phys. J. C **61**, 311 (2009).
- [54] L.S. Geng, J. Martin Camalich, M.J. Vicente Vacas, Phys. Rev. D **80**, 034027 (2009).

- 315 [55] C. Alexandrou, T. Korzec, G. Koutsou, J.W. Negele, and Y. Proestos, Phys. Rev. D **82**, 034504 (2010).
316 [56] G. Ramalho and M.T. Peña, Phys. Rev. D **83**, 054011 (2011).
317 [57] C.J. Batty, E.Friedman, and A. Gal, Phys. Rev. C **59**, 295 (1999).
318 [58] E. Friedman, A. Gal, Phys. Rep. **452**, 89 (2007).
319 [59] L.W. Alvarez, Phys. Rev. D **8**, 702 (1973).
320 [60] W.F. Fry, J. Schneps, and M.S. Swami, Phys. Rev. **97**, 1189 (1955).
321 [61] Y. Eisenberg, Phys. Rev. **96**, 541 (1954).
322 [62] V.E. Barnes *et al.*, Phys. Rev. Lett **8**, 204 (1964).
323 [63] A.B. Kaidalov, P.E. Volkovitsky, Z. Phys. C **63**, 517 (1994).
324 [64] J. Pochodzalla, Phys. Lett. B **669**, 306 (2008).
325 [65] J. Pochodzalla, Hyperfine Interact. **194**, 255 (2009).
326 [66] A. Sanchez Lorente, S. Bleser, M. Steinen, J. Pochodzalla, Phys. Lett. B **749**, 421 (2015).
327 [67] A.B. Larionov, I.A. Pshenichnov, I.N. Mishustin, W. Greiner, Phys.Rev.C **80**, 021601 (2009).